Research Paper

Study on Mechanism and Suppression Method of Flow-Induced Noise in High-Speed Gear Pump

Peng ZHAN, Yan QIANG, Zhiyuan JIANG, Runxue YANG, Liejiang WEI*

Energy and Power Engineering College, Lanzhou University of Technology
Qilihe District, Lanzhou, Gansu Province, P.R. China

*Corresponding Author e-mail: weiliejiang@126.com

The flow-induced noise mechanism of a 5000 rpm high-speed gear pump is explored. On the basis of the CFD technology and the Lighthill acoustic analogy theory, a numerical model of the flow-induced noise of a high-speed gear pump is constructed, and the effect of oil suction pressure (0.1–0.2 MPa) on the internal flow field and flow-induced noise characteristics of the high-speed gear pump is investigated. To evaluate the accuracy of the numerical simulation, a noise testing platform for high-speed gear pumps was developed. Adding an oil replenishment groove to the high-speed gear pump suppresses its flow-induced noise. The results indicate that the discrete noise at the fundamental frequency and its harmonic frequency is the primary component of the flow-induced noise of the pump and that the oil-trapped area is the principal source of vibration. The overall sound pressure level of flow-induced noise in the inlet and outlet areas decreases with distance from the oil-trapped area, and the sound pressure level in the outlet area is greater than that in the inlet area. The oil replenishment groove may considerably minimize cavitation noise, enhance the oil absorption capacity, and reduce the outer field's overall sound pressure level by 4–5 dB.

Keywords: external gear pumps; flow-induced noise; the oil replenishment groove; flow pulsation rate.

1. Introduction

In volumetric pumps, gear pumps are widely used as power units in hydraulic systems due to their simple structure, strong anti-fouling ability, and low price. With the development of high-speed and high-pressure gear pumps, the problem of high noise induced by working is becoming more and more obvious (Woo, Vacca, 2020). The noise of the gear pump is composed of mechanical noise and flow-induced noise. The research shows that flow-induced noise is the major source of noise in high-speed gear pumps, which is mainly composed of cavitation noise, flow pulsation noise, oil-trapped noise, and turbulent noise (Fiebig, Wróbel, 2022). The mechanical vibration noise can be suppressed or eliminated by improving the processing and manufacturing accuracy, and there is research on the noise decomposition analysis (Wang *et al.*, 2016a). The flow-induced noise is due to its complex

sound generation mechanism, the wide range of frequency involved, and the profound degree of harm, that we must pay attention to. The working speed of the gear pump is an important factor affecting its working stability. Excessive speed will aggravate the occurrence of cavitation and the phenomenon of trapped oil, causing serious vibration noise (Woo, Vacca, 2022). However, too low a speed will cause a low volumetric efficiency of the gear pump. Therefore, the working speed is usually set in the range of 600–3000 r/min. The high-speed gear pump studied in this topic has a high speed (3000–5000 r/min) and low oil suction pressure under actual working conditions. On the one hand, it is difficult for the oil to fill the tooth groove in time due to the centrifugal force generated by the high speed, resulting in serious gas accumulation at the tooth root and reducing the volumetric efficiency of the pump. Furthermore, it will also aggravate the cavitation of the pump and produce serious

cavitation noise (Zhang *et al.*, 2021). Therefore, flow-induced noise is the main component of high-speed gear pump noise.

In this paper, the mechanism of flow-induced noise of a high-speed gear pump with a speed of 5000 r/min is analyzed. Based on the CFD technology and the Lighthill acoustic analogy theory, a numerical model of the flow-induced noise of a high-speed gear pump is established. The variation characteristics of internal and external sound fields of flow-induced noise of gear pumps at different speeds are studied. The noise test system of the high-speed gear pump is built to verify the accuracy of numerical simulation. Finally, the flow-induced noise suppression effect of the high-speed gear pump is achieved by adding an oil replenishment groove.

2. Mechanism analysis of flow-induced noise in high-speed gear pump

Flow-induced noise and mechanical noise are important sources of gear pump noise. With the development of a high-speed gear pump and the improvement of machining accuracy, flow-induced noise will be much greater than mechanical noise. The specific causes are summarized as follows.

2.1. Cavitation noise

For the operation of rotating machinery with fluid as the working medium, the occurrence of cavitation is often accompanied. When the fluid flows through the variable cross-section channel, the flow rate of the fluid will increase and the pressure will decrease. When the local fluid pressure is lower than the saturated vapor pressure of the oil, the gas incorporated in the oil will be vaporized and precipitated. The precipitated gas is brought to the high-pressure area by the oil. When the bubble is shattered while it is being subjected to pressure, it will generate a strong pressure in the core of the bubble, which will lead to a huge impact and a lot of noise, specifically cavitation noise (Liu *et al.*, 2015; 2016).

2.2. Oil trapped noise

In order to ensure the normal operation of involute gears, the contact degree of gear meshing is required to be greater than 1, so there is an inevitable trapped oil volume. When the oil in the trapped oil volume is squeezed by the rotation of the gear, the compressibility of the oil is very small, and the oil in the trapped oil area will produce strong hydraulic impact and extrusion leakage, which will cause vibration and noise of the gear and the pump. At the same time, when the volume of the trapped oil area changes from small to large, it will induce cavitation and aggravate noise pollution (Guo, Guan, 2021).

2.3. Flow pulsation noise

As a kind of volumetric pump, the working principle of the gear pump inevitably produces periodic flow changes due to the structural characteristics, which makes the discharged oil to exhibit periodic flow pulsation. The flow pulsation at the outlet will cause pressure pulsation under the coupling with the load, which can cause vibration and noise of gear pumps, pipelines, and other components of the system. If the frequency of the flow pulsation coincides with a certain frequency of the system, it will also cause resonance and produce stronger noise (Marinaro *et al.*, 2021).

2.4. Turbulent noise

When the gear pump works, the internal fluid flow law is complex, and the fluid flow is more disordered under high-speed working conditions, thus inducing strong noise, that is, turbulent noise, which is usually composed of a turbulent boundary layer and its wake, vortex shedding from the solid surface, turbulence impacting the solid surface and other factors, and the spectrum presents a broadband characteristic.

The flow-induced noise of a high-speed gear pump is primarily caused by the unsteady flow of its internal fluid. From the perspective of the generation mechanism of flow-induced noise, the types of fluid sound sources can generally be divided into monopole sources, dipole sources, and quadrupole sources. Figure 1 shows the sound source models and characteristics of three kinds of fluid sound sources (Wang *et al.*, 2016b). Among them, Ma represents the Mach number, Wa refers to sound radiation velocity, and U_0 represents sound radiation velocity without disturbance.


Point power name	Source power	Flow field	Slow field	Radiation efficiency
Single-level sub	Volume fluctuation			$(Wa/U_0)Ma$
Even-level sub	Center-of-mass oscilation			$\frac{1}{2}(Wa/U_0)^3 Ma^3$
Fourth-level sub	Shearing stress			$\frac{1}{27}(Wa/U_0)^5 Ma^5$
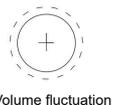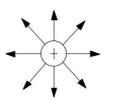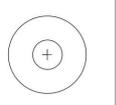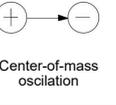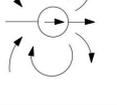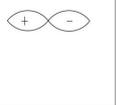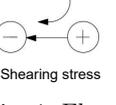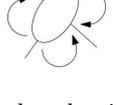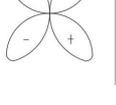
Fig. 1. Flow-induced noise source model and its characteristics.

The monopole source can be considered a point source of pulsating mass flow, which is mainly caused by the uneven mass or heat inflow in the medium.

The intensity of the sound source is proportional to the square of the Mach number. The dipole source can be regarded as the composition of two anti-phase monopole sources. The main reason is the interaction between the fluid and the solid contact with it. The intensity of the sound source is proportional to the third power of the Mach number, and the directivity of the sound radiation presents the "8" shape. The spectrum presents discrete characteristics. The common dipole source noise includes the boundary layer noise and the propeller rotation noise. Quadrupole sources can be considered to be composed of two anti-phase dipole sources, which are mainly produced in the stress change of turbulent fluid. The intensity of the sound source is proportional to the fifth power of the Mach number, and the directivity of acoustic radiation is a "four lobes" shape. The spectrum shows broadband characteristics. The common four-level sub-source noise includes jet noise and turbulent noise. From the perspective of noise radiation efficiency, the highest to lowest radiation intensity are: the monopole source, the dipole source, and the quadrupole source.

The flow-induced noise of the high-speed gear pump is composed of the above three fluid sound sources, in which the cavitation noise belongs to the monopole source noise. Since the high-speed rotation of the gear intensifies the occurrence of cavitation, and the radiation efficiency of the monopole source noise is higher than that of the other two sound sources, the monopole source noise is often a key factor in the noise reduction of the high-speed gear pump. The vibration radiation noise of the pump body contacted by the pressure fluctuation of the fluid belongs to the dipole source noise. Although the noise radiation efficiency is not as good as that of the monopole source noise, it often forms a strong noise level. Turbulent noise belongs to the fourth-order sub-source noise. Because its noise radiation efficiency is the weakest and is often considered at a high Mach number, the fluid flow in a high-speed gear pump belongs to a low Mach number, so it is ignored.

3. Numerical simulation

3.1. Calculation model

Since the involute gear is easy to manufacture and has a strong bearing capacity, the object of this study is designed as the involute external gear pump. The theoretical displacement of the pump is 72 mL/r, the working pressure is 2 MPa, and the working speed is 3000–5000 r/min. The simplified geometric modeling of the gear pump is carried out in Creo software, which is mainly composed of an inlet, an upper pump cover, a lower pump cover, a gear, and a floating side plate, as shown in Fig. 2. The main geometric parameters of the gear part of the external gear pump calculated ac-
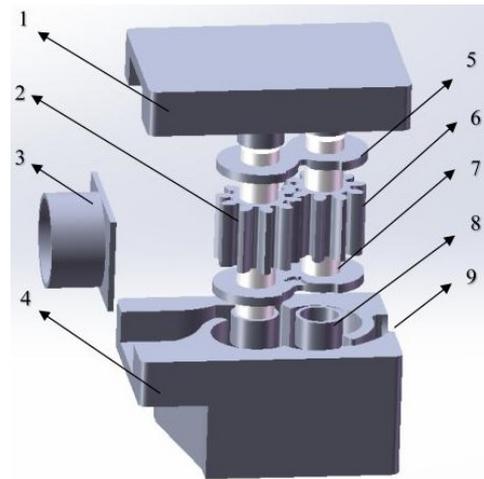

Fig. 2. Structure diagram of high-speed gear pump: 1) upper pump cover; 2) driving gear; 3) inlet; 4) lower pump cover; 5) floating side plate; 6) driven gear; 7) pump shaft; 8) needle roller bearing; 9) outlet.

cording to the design parameters are shown in Table 1. The diameter of the oil suction port of the gear pump is 58 mm, and the diameter of the oil discharge port is 30 mm.

Table 1. Gear design parameters.

Parameter	Parameter value
Module of gear	5
Tooth number	10
Gear indexing circle diameter [mm]	50
Addendum [mm]	4
Tooth dedendum [mm]	7.25
Root diameter [mm]	35.5
Addendum circle diameter [mm]	58
Pressure angle [°]	20
Displacement factor	−0.2
Operating center distance [mm]	47.5
Tooth width [mm]	45

3.2. Flow field calculation

Based on the Pumplinx flow field analysis software, the internal flow field of the gear pump was simulated and analyzed. The SIMPLEC algorithm was used, and the RNG k-ε turbulence model was used for the turbulence model. This model was an important correction based on the standard k-ε turbulence model. By reflecting the influence of small-scale vortex in the corrected viscosity term and large-scale vortex motion, this model can calculate the low Reynolds number turbulence and take into account the vortex effect, which improves the calculation accuracy of strong vortex flow (CHEN *et al.*, 2003). The grid division of the computational model adopts the special grid generator template provided by software. The final number of grid cells

is 462761, and the number of grid nodes is 1486231. The overall grid division is shown in Fig. 3.

a)   b)
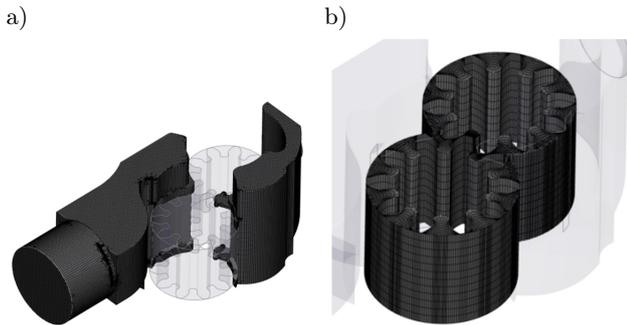
Fig. 3. Grid model of flow field: a) import and export areas; b) gear region.

In this paper, the residual convergence accuracy of the simulated physical quantity is set to 0.1, the time step of each tooth is set to 40 steps, the number of teeth is 10, and the gear is set to rotate for 10 rotations. Then the total time step is 4000. At the same time, to ensure the accuracy of the subsequent acoustic simulation, the flow field data showing periodic changes in the next five rotations are exported as the sound source term of the acoustic calculation with the En-Sight format file. Table 2 shows the specific settings of simulation boundary conditions.

Table 2. Boundary conditions and parameter settings.

Dynamic viscosity [Pa·s]	0.2532516
Fluid density [kg/m^3]	860
Elasticity of modulus of liquid bulk [Pa]	2.15e + 09
Saturated vapor pressure [Pa]	37100
Initial gas content	0.00009
Temperature [°]	20
Inlet pressure [MPa]	0.1, 0.15, 0.2
Outlet pressure [MPa]	2
Revolution speed [r/min]	3000, 4000, 5000

3.3. Sound field calculation

In this paper, the acoustic simulation of the flow-induced noise of the external gear pump is carried out based on the acoustic finite element method and the infinite element method. The body sound source and surface sound source of the fluid are extracted by the CAA method and interpolated into the corresponding acoustic body grid and the surface grid. Then, the noises generated by the flow field are simulated and their sound pressure spectra were obtained (CARLETTI *et al.*, 2016). To improve the accuracy of acoustic calculation, acoustic modeling only retains the important structural characteristics of the high-speed gear pump, the structural mesh of the pump body only retains the upper and lower pump covers, does not include gear and bearing and other parts, and the bearing holes

are closed. The acoustic calculation model is mainly composed of body sound source, surface sound source, sound propagation area, and acoustic infinite element (PASZKOWSKI, 2020). The grid model is established in HyperMesh software and the material properties of different components are defined, as shown in Fig. 4.

a)

b)
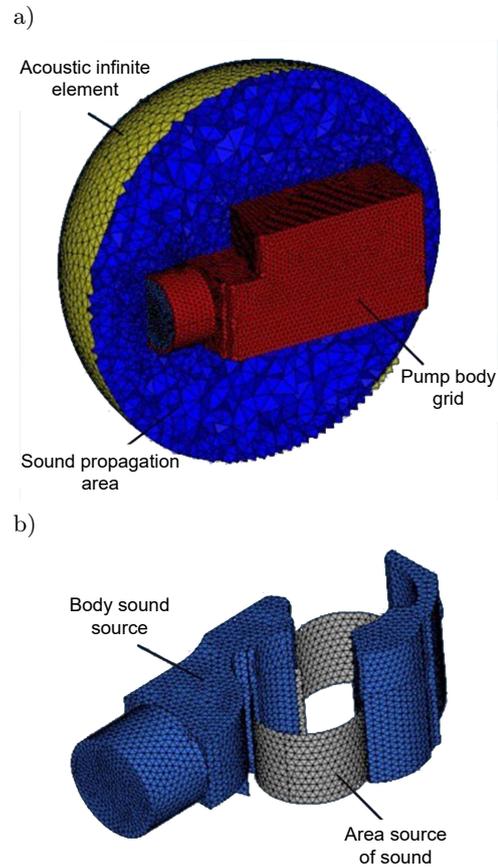
Fig. 4. Acoustic grid model: a) pump body and acoustic finite element infinite element mesh; b) acoustic grid in fluid domain.

Due to the consideration of the external radiation of the fluid sound source, the acoustic grid must include the grid of the external air domain, and the interface of each part of the grid is set as a common node, so that the transmission of acoustic information between various components can be realized. The size of the acoustic mesh is determined by the analysis frequency of the fluid. The maximum size $L_{\max}$ of the acoustic mesh should be calculated:

$$L_{\max} < c/6f_{\max}. \qquad (1)$$

In the aforementioned equation, the sound speed c is about 1300 m/s, and the time step Δt of flow field calculation under each speed condition is 5×10^{-5} s, 3.75×10^{-5} s, and 3×10^{-5} s, respectively. Then the maximum frequency $f_{\max}$ at three speeds can be calculated by the sampling law, and the maximum frequency $f_{\max}$ is 16 666 Hz. Therefore, the maximum

size $L_{\max}$ of the acoustic grid should be less than 13 mm, and the maximum size of the acoustic grid of each part of the high-speed gear pump should not exceed 0.2 mm, which can fully meet the requirements of the acoustic calculation. When converting time-domain acoustic information to frequency-domain acoustic information with a fast Fourier transform, the window function needs to be set as a Hanning window to reduce signal leakage. To explore the frequency response characteristics of the fluid sound source inside the high-speed gear pump, three monitoring points are set in the inlet and outlet areas of the pump, as shown in Fig. 5.
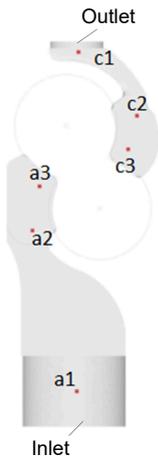
Fig. 5. Internal acoustic monitoring points.

4. Analysis of numerical simulation results

4.1. Analysis of flow field calculation results

Figure 6 depicts the flow pulsation curve of the high-speed gear pump outlet under each oil suction pressure after periodic stable fluctuation. From the information in the graph, it can be seen that the instantaneous flow curve of each graph shows periodic change, which conforms to the essence that the periodic change of the meshing point position leads to the periodic change of the output flow. With the increase of the rotational speed, the amplitude of outlet flow pulsation is stronger. When the oil suction pressure is 0.1 MPa, the fluctuation amplitude of the outlet flow pulsation of the high-speed gear pump is large under various rotational speeds. With the increase of the oil suction pressure, the amplitude of the outlet flow pulsation decreases gradually. The main reason is that the increase of the oil suction pressure inhibits the cavitation level in the gear rotor area, resulting in the decrease of the flow pulsation at the outlet. Therefore, the way of pressurizing the oil tank pressure can be used to reduce the occurrence of internal cavitation in high-speed gear pumps and to reduce the cavitation noise level.
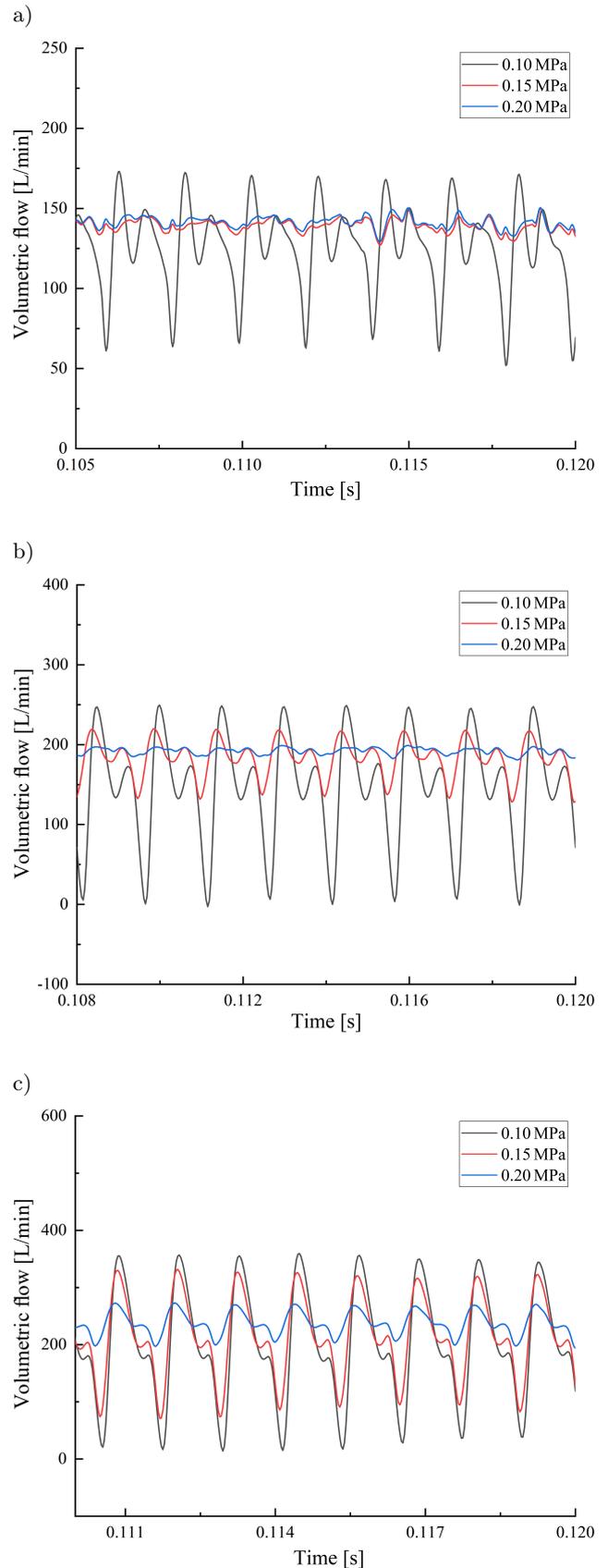

Fig. 6. Fluctuation curve of outlet flow under each suction pressure: a) 3000 r/min; b) 4000 r/min; c) 5000 r/min.

4.2. Analysis of sound field calculation result

After the acoustic calculation is completed, the distribution cloud diagram of surface and body sound sources at the fundamental frequency and its harmonics are selected. From the formula $f = n \cdot Z/60$, it can be seen that when the rotational speed is 4000 r/min, the passing frequency (fundamental frequency) of the gear to the fluid is 667 Hz, and then 1333, 2002, and 2665 Hz are all harmonics of the fundamental frequency (Huang *et al.*, 2019). From Fig. 7 the distribution of surface sound sources and sound pressure levels at different locations can be seen. In the distribution of the surface sound source on the outer wall of the gear rotation area, the alternating occurrence of the maximum and minimum sound pressure levels is the discrete sound source when the high-speed gear pump works. Compared with other frequencies, the sound pressure level at the fundamental frequency is the highest, and with the increase of frequency, the sound pressure level shows a significant decreasing trend.
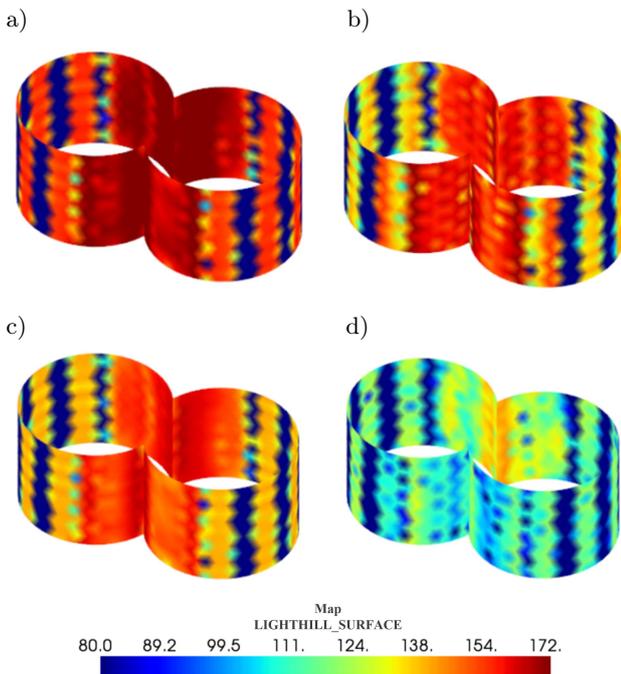

Fig. 7. Surface sound source images at fundamental frequency and harmonics frequency [dB]: a) 667 Hz; b) 1333 Hz; c) 2002 Hz; d) 2665 Hz.

It can be seen from the distribution cloud diagram of the body sound source in Fig. 8 that the sound pressure level of the body sound source is much higher than that of the surface sound source. The sound pressure level of the body sound source at the fundamental frequency is the highest, and with the increase of frequency, the sound pressure level also shows a significant decreasing trend. The sound pressure level in the outlet area is higher than that in the inlet area because the oil in the outlet area is subjected to a high-pressure load and has a strong impact on the pump body, which makes the sound pressure level relatively high. In addition, the sound pressure level at the junction of the gear and inlet and outlet fluid domain is also high. The unstable flow will produce obvious turbulence and vortex phenomena, and the fluctuation of oil pressure directly affects the level of the sound pressure.
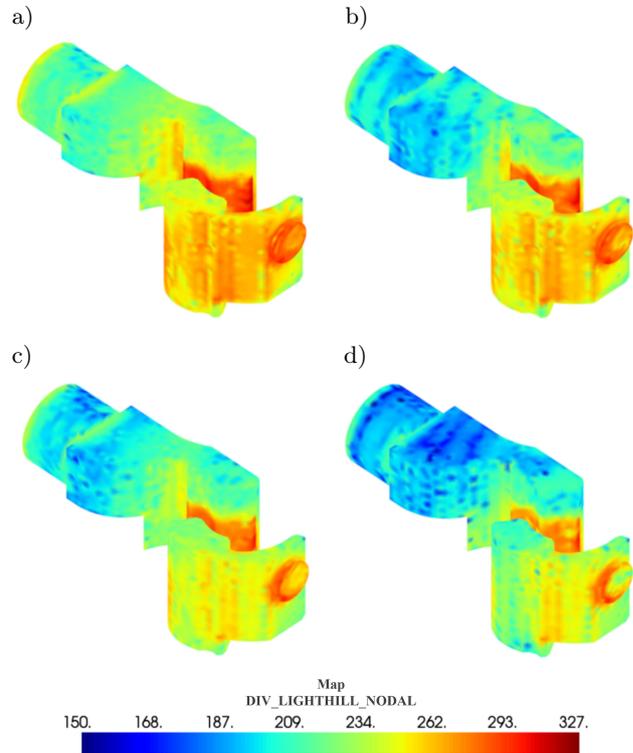

Fig. 8. Cloud images of body sound source at fundamental frequency and its harmonics frequency [dB]: a) 667 Hz; b) 1333 Hz; c) 2002 Hz; d) 2665 Hz.

Figure 9 shows the flow-induced noise spectrum curves of each acoustic monitoring point at the inlet and outlet under the working condition of 4000 r/min. It can be found that the sound pressure level spectrum is mainly composed of wideband noise and discrete noise. The peak value of the sound pressure level appears at the fundamental frequency (667 Hz) and harmonics frequency (1333, 2002, 2665 Hz). The sound pressure levels at the fundamental frequency and harmonics frequency are about 10–20 dB higher than those at other frequency bands, indicating that the flow pulsation formed by the periodic mutual force between the gear and the fluid is the key factor to induce the flow-induced noise.

The total sound pressure level of the inlet region is 182–199 dB, while the total sound pressure level of the outlet region is 195–212 dB. The total sound pressure level of the outlet region is higher than that of the inlet region, and the total sound pressure level of the import and export monitoring points decreases with the gear rotor area to the import and export sides.
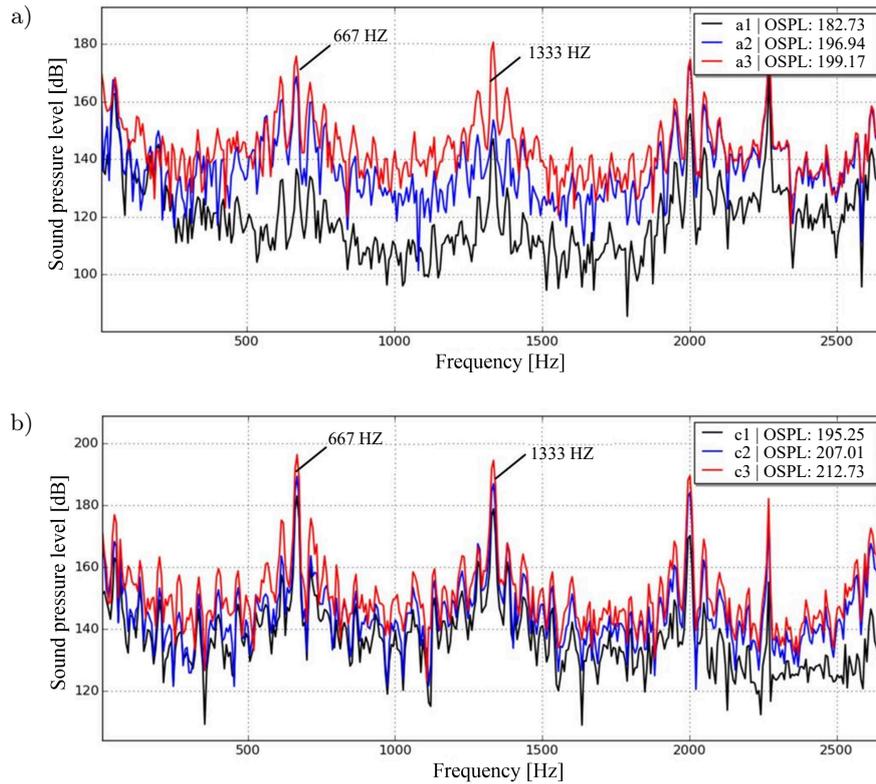
Fig. 9. Spectrum of sound pressure level in pump: a) imported spectrum curve; b) export spectrum curve.

Table 3 shows the summary of the total sound pressure levels at the inlet and outlet of the high-speed gear pump under different oil suction pressures. It can be found that the total sound pressure level in the internal fluid domain increases with the increase of the rotational speed. The total sound pressure level in the outlet area is much higher than that in the inlet area, and the total sound pressure level in the inlet and outlet area decreases with the increase of the oil suction pressure. The main reason is that the increase of the oil suction pressure can reduce the gas content of the oil, improve the effective volume elastic modulus of the oil, and reduce the compressibility of the oil, thus

greatly inhibiting the occurrence of cavitation under high-speed conditions. Comparing the change of the total sound pressure level at the monitoring point a2 in the import area with that at the point c2 in the export area, it can be found that for every 0.05 MPa increase in the oil absorption pressure, the total sound pressure level at the monitoring point a2 in the import area decreases by 3–8 dB, while the total sound pressure level at the monitoring point c2 in the export area decreases by 10–14 dB, indicating that the noise reduction effect of increasing the oil absorption pressure in the export area is better than that in the import area.

5. Experimental verification

5.1. Experimental system

Due to the complex generation mechanism of flow-induced noise of a high-speed gear pump, it is often difficult to convincingly study the results only by numerical simulation. Therefore, to verify the accuracy of the above acoustic simulation, this section carried out the noise test experiment of the high-speed gear pump. The noise test experiment of the high-speed gear pump is carried out on the hydraulic system test bench of the oil pump production workshop in Dongguan. The experimental system mainly includes a gear pump operation system and a data acquisition system. The gear pump operation system includes a gear

Table 3. Total sound pressure level table of import and export monitoring points under oil suction pressure.

Revolution speed [r/min]	Suction pressure [MPa]	a2 total sound pressure level [dB]	c2 total sound pressure level [dB]
3000	0.1	191	200
	0.15	182	189
	0.2	179	185
4000	0.1	197	207
	0.15	189	195
	0.2	187	187
5000	0.1	205	217
	0.15	196	203
	0.2	193	192

pump, drive motor, pressure regulating valve, pipeline, sound insulation cover, and oil tank. The data acquisition system collects various physical quantities in the operation of a high-speed gear pump with the help of an acquisition instrument and various sensors, including a sound pressure sensor, turbine flowmeter, photoelectric speed meter, pressure gauge, and thermometer. The experimental system is shown in Fig. 10.
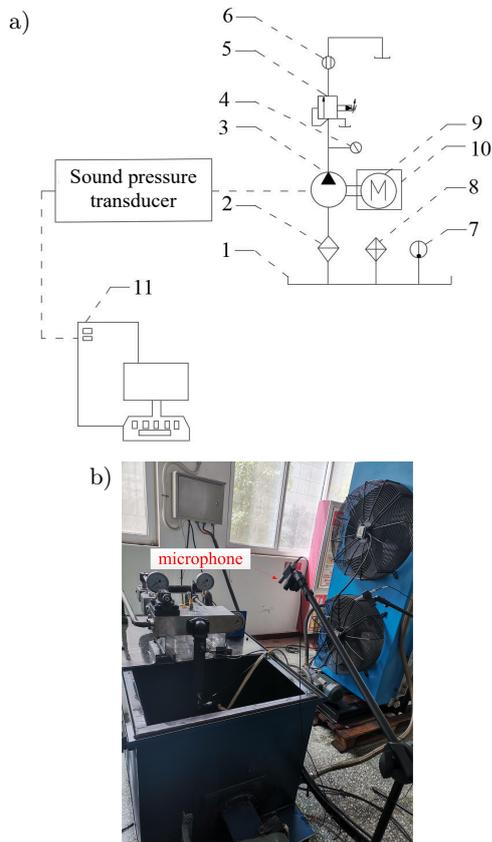

Fig. 10. Experimental system diagram: a) system schematic diagram (1 – tank; 2 – filter; 3 – gear pump; 4 – pressure gauge; 5 – pressure regulating valve; 6 – flowmeter; 7 – thermometer; 8 – heater; 9 – sound insulation cover; 10 – motor; 11 – data acquisition system); b) physical figure.

The acquisition instrument used in this experiment is the INV3062SC series 24-bit network distributed acquisition instrument of the Beijing Oriental Institute of Vibration and Noise. The sound pressure sensor adopts the IEPE microphone preamplifier of the Beijing Oriental Institute, which belongs to capacitive testing sensors. The frequency response range is 16 Hz–100 kHz, the measurement accuracy is ±0.5 dB, the maximum output voltage can reach 5.0 V_{rms}, and the working condition is −40 to 85°C. The dynamic measurement of the sound pressure sensor can ensure that the total distortion of the sound pressure level below 146 dB is not more than 3%. In order to record the noise generated by the high-speed gear pump, the sampling frequency of the experimental test is 8 kHz, and the sampling time is 90 s. After the sampling is completed,

the time-frequency conversion window function of the acoustic signal is set as the Hanning window.

5.2. Comparison between experimental results and simulation

In this noise sampling, to prevent the noise signal generated during the operation of the driving motor from affecting the experimental results, the motor is wrapped by sound absorption materials. The arrangement of acoustic pressure sensors refers to the relevant standards (Tang *et al.*, 2014). The acoustic pressure sensors are arranged according to the hemispherical method and make appropriate adjustments according to the actual situation of the site. Due to the small volume of the gear pump in this experiment, the length, width, and height of the pump body are all less than 0.5 m, and the radius of the hemisphere should not be less than twice the length of the experimental object and not less than 1 m. Therefore, the sound pressure sensor arranged at a radius of 1 m from the pump source. In this experiment, three acoustic measuring points were placed around the outlet of the radial section of the gear pump and measured synchronously. Each measuring point is 1 m away from the gear pump, and the three measuring points are sandwiched by 40°. The actual measurement point arrangement is shown in Fig. 11.
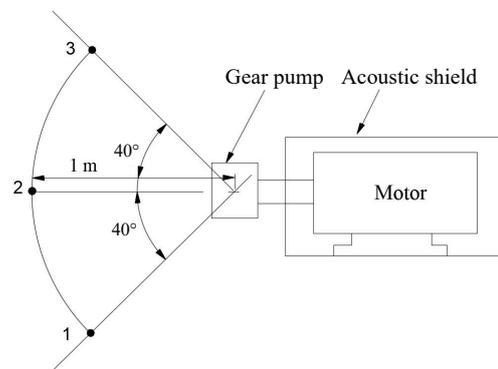

Fig. 11. Arrangement of sound pressure sensor measurement points.

The fast Fourier transform (FFT) is performed on the time domain information of the noise of the sampled high-speed gear pump to obtain the sound pressure level spectrum of the noise. Figure 12 is the comparison between the experimental values and the simulation values of three acoustic measuring points. Due to the error of the practical test and the numerical simulation itself, the experimental values are higher and lower than the simulation values in each frequency band, but the overall trend is the same. The discrete noise of the practical and simulation values is pronounced at the fundamental frequency and harmonics frequency. The experimental values of the three acoustic measuring points are slightly larger than the simula-

a)

b)

c)
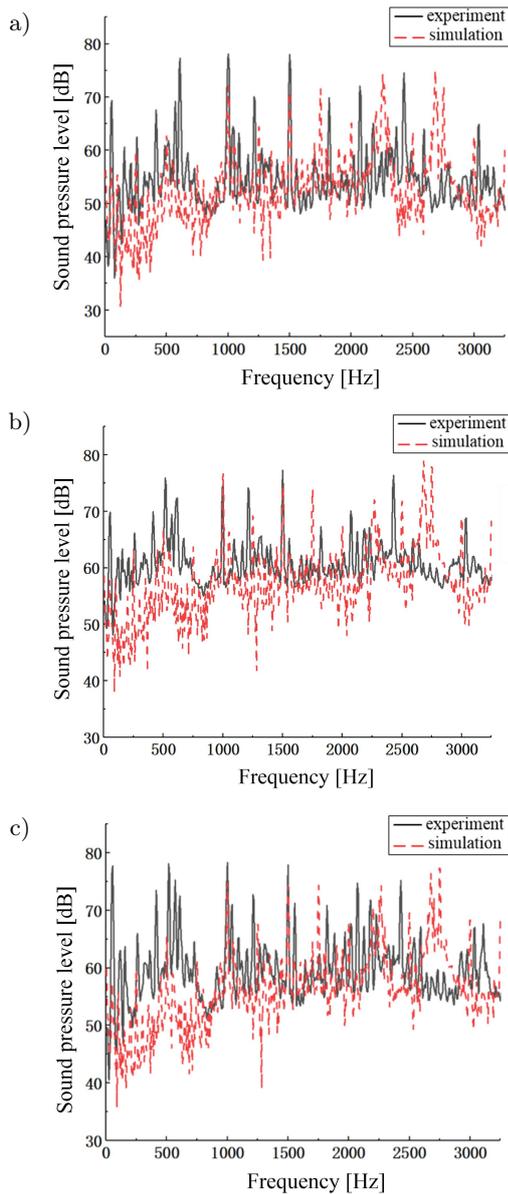
Fig. 12. Spectrum comparison of sound pressure level: a) measurement point 1; b) measurement point 2; c) measurement point 3.

tion values in the range of 0–1000 Hz. The experimental values are in good agreement with the simulation values at the second frequency (1000 Hz) and the third frequency (1500 Hz). Since the influence of the mechanical noise of the pump, actual measured noise is more than that of the simulated noise spectrum.

At 3000, 4000, and 5000 r/min measured experimentally, the average sound pressure levels considering A-weighting are 87, 90, and 94 dB, respectively. Table 4 compares the experimental and simulation noise values at each measuring point noise characteristic of 3000 r/min. According to the table, the noise value measured by the experiment is slightly higher than the simulation value because the noise measure-

ment of the high-speed gear pump cannot exclude mechanical noise interference. However, the maximum error of the noise value obtained by experiment and simulation is less than 7 dB at each frequency. The feasibility of the algorithm used in this paper to simulate the flow-induced noise of a high-speed gear pump is demonstrated within an acceptable range.

Table 4. Experimental simulation comparison of noise values at characteristic frequencies [dB].

Frequency [Hz]		500	1000	1500
Measuring point 1	Experiment	76	75	78
	Simulation	69	76	75
	Error	7	1	3
Measuring point 2	Experiment	79	79	79
	Simulation	73	76	76
	Error	6	3	3
Measuring point 3	Experiment	78	79	78
	Simulation	72	75	74
	Error	6	4	4

6. Simulation analysis of noise reduction optimization

6.1. Structure design of oil replenishment tank

Under actual operating conditions, the high-speed gear pump in this paper has a low oil suction pressure. On the one hand, due to the centrifugal force, it is difficult for the oil to fill the grooves in time, resulting in the accumulation of gas in the oil at the root of the tooth, which severely reduces the volumetric efficiency of the pump. On the other hand, it will cause cavitation to become more intense. The precipitated gas flows to the high-pressure area of the outlet and collapses with the rotation of the gear, producing a loud cavitation noise. As a result, Gianluca Marinaro proposed a side plate structure that controls the reverse flow to achieve a consistent reduction in the amplitude of flow unevenness (Zhou *et al.*, 2018).

A scheme for opening an oil replenishment groove near the inlet side of the floating side plate is proposed in this paper. In time, the oil can be added to the tooth groove. The inner diameter (d = 35.5 mm) and outer diameter (D = 46.75 mm) of the oil replenishment groove are designed as the diameter of the tooth root circle and the diameter of the dividing circle, respectively, to improve the filling effect of the oil. Figure 13 depicts the structure of the floating side plate.

To find the best angle and depth of the oil replenishment tank, the angle of the oil replenishment tank in this simulation is interpolated once every 5° from 120° to 250°, and the angle of the two teeth in the high-pressure area is retained for oil sealing. The depth of the oil replenishment tank is set as a group from 0.4 to 4 mm every 0.4 mm. To analyze the influence of oil re-
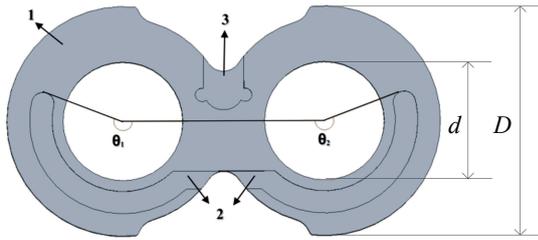
Fig. 13. Structure of oil tank: 1) side plate; 2) oil filling groove; 3) unloading groove.

plenishment tank structure on the flow-induced noise of the high-speed gear pump, the outlet flow pulsation rate under each oil suction pressure is calculated according:

$$\delta = \frac{Q_{\max} - Q_{\min}}{Q_{\mathrm{avg}}}, \qquad (2)$$

where δ is the flow pulsation rate; $Q_{\max}$ is the maximum value of instantaneous flow; $Q_{\min}$ is the minimum value of instantaneous flow; Q_{avg} is the average flow value, L/min. Figure 14 depicts the variation curve of
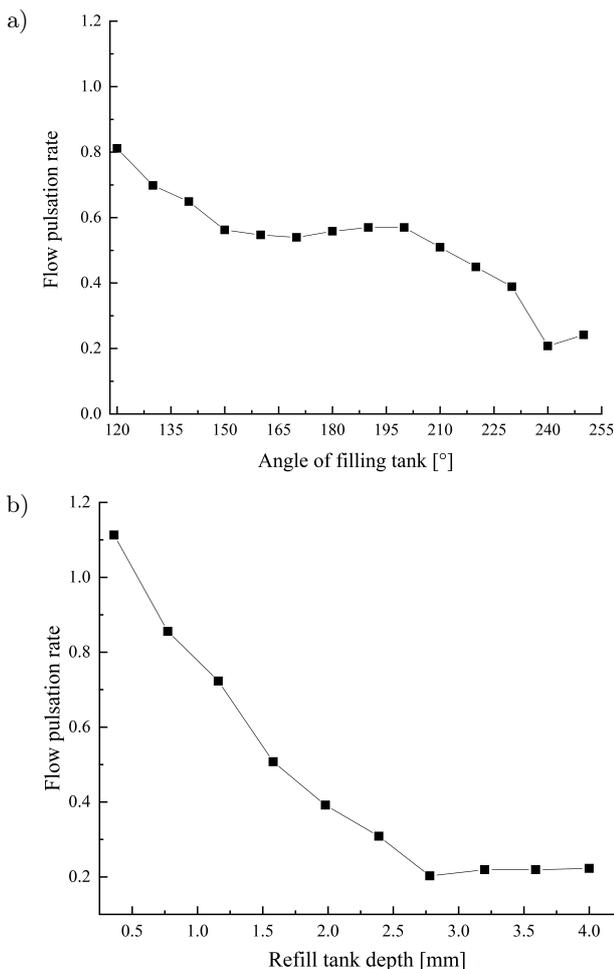

Fig. 14. Variation curve of flow pulsation rate – the relationship between flow pulsation rate and: a) the angle of oil feeding tank; b) tank depth.

the gear pump's outlet flow pulsation rate with the angle and depth of the oil replenishment tank.

Through the analysis of Fig. 14a, it can be seen that the fluctuation rate of the outlet flow of the high-speed gear pump changes gently before 240°. At 240°, the fluctuation rate of the outlet flow decreases sharply. Therefore, in order to avoid the decrease of the volumetric efficiency caused by too large an angle in the design of the oil replenishment tank, 240° is the best choice. Figure 14b shows that the flow pulsation rate at the outlet shows a decreasing trend before the oil replenishment tank depth is 2.8 mm. When the tank depth is greater than 2.8 mm, the flow pulsation rate tends to be gentle. Considering the structural strength problem caused by the deep oil tank, the selection of the oil replenishment tank with 2.8 mm depth in the design has the best effect on reducing the noise caused by the flow pulsation.

6.2. Simulation comparison after optimization

The flow field calculation results with the oil replenishment tank structure are loaded into acoustic software to calculate flow-induced noise. After the calculation, a section is set in the axial and radial directions of the original pump and the improved pump, respectively, to show the change in the sound pressure level of the external field before and after the improvement. The sound radiation slice nephograms before and after the improvement at the fundamental frequency are selected, as shown in Fig. 15. Table 5 summarizes the total sound pressure level summary of the external acoustic monitoring points after the modification.
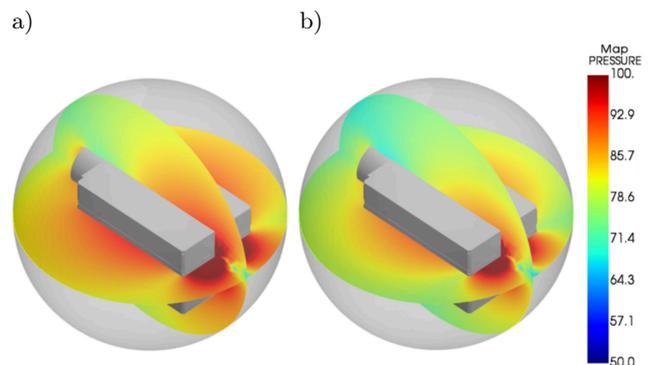

Fig. 15. Acoustic radiation slice images at fundamental frequency: a) original pump; b) improvement.

As demonstrated in Fig. 15, the sound pressure level in the external field of the modified high-speed gear pump is significantly lower than that of the original pump. The statistics in Table 5 show that the high-speed gear pump with the oil replenishment groove construction has a lower external sound pressure level than the original pump, and the total sound pressure level is reduced by 4–5 dB. As a result, the cavitation

Table 5. Comparison of total sound pressure level before and after improvement of external measuring points [dB].

Revolution speed [r/min]		3000	4000	5000
Measuring point 1	Original	88	91	94
	Improvement	83	86	90
Measuring point 2	Original	87	90	94
	Improvement	82	87	90
Measuring point 3	Original	89	91	95
	Improvement	84	86	91

and flow pulsation levels in the pump can be lowered by opening the oil replenishment groove on the floating side plate near the gear side. As a result, the level of flow-induced noise caused by oil flow is reduced.

7. Conclusions

In this research, the CFD method and the Lighthill sound analogies theory are utilized to develop a calculation model of flow-induced noise of an external gear pump that accurately reflects the internal flow noise characteristics of the external gear pump. The findings indicate:

1) The experimental and simulation results show that the spectrum curves of the external sound pressure level of the high-speed gear pump measured in the experiment agree well with the simulation, and the maximum error of the noise value at the characteristic frequency is less than 7 dB, confirming the accuracy of the numerical simulation.

2) The flow-induced noise of the high-speed gear pump is dominated by discrete noise at the fundamental frequency and its harmonics frequency. The intensity of cavitation and flow-induced noise in the internal fluid region decreases as oil suction pressure increases, and the noise reduction effect in the outlet zone is greater than that in the inlet region. The main source of vibration is the oil trapped zone. The overall sound pressure level of flow-induced noise decreases with distance from the oil trapped zone in the inlet and outflow regions, and the sound pressure level in the outlet region is higher than that in the inlet region.

3) The effect of minimizing the flow pulsation rate at the output of the high-speed gear pump is optimal when the planned oil replenishment tank angle is approximately 240° and the depth is about 2.8 mm. The simulation shows that increasing the size of the oil replenishment tank can significantly reduce the intensity and range of cavitation in the pump, improve oil absorption ability, and reduce total sound pressure level in the external field by about 4–5 dB, achieving the flow-induced noise suppression effect.

References

1. CARLETTI E., MICCOLI G., PEDRIELLI F. (2016), Vibroacoustic measurements and simulations applied to external gear pumps. An integrated simplified approach, *Archives of Acoustics*, **41**(2): 285–296, doi: 10.1515/aoa-2016-0028.

2. CHEN Q.G., XU Z., ZHANG Y.J. (2003), Application of RNG K-ε model in numerical calculation of engineering turbulence [in Chinese], *Chinese Quarterly Journal of Mechanics*, **24**(1): 88–95.

3. FIEBIG W., WRÓBEL J. (2022), Experimental and numerical investigation on the noise development in fluid power units: An overview, *Archives of Civil and Mechanical Engineering*, **22**(4): 1–18, doi: 10.1007/S43452-022-00481-X.

4. GUO S.X., GUAN X.F. (2021), Simulation research on trapped oil pressure of involute internal gear pump, *Mathematical Problems in Engineering*, **2021**: 8834547, doi: 10.1155/2021/8834547.

5. HUANG P.L. *et al.* (2019), A study on noise reduction of gear pumps of wheel loaders based on the ICA model, *International Journal of Environmental Research and Public Health*, **16**(6): 999, doi: 10.3390/ijerph16060999.

6. LIU Y.Y., WANG L.Q., ZHU Z.C. (2015), Numerical study on flow characteristics of rotor pumps including cavitation, *Proceedings of the Institution of Mechanical Engineers, Part C: Journal of Mechanical Engineering Science*, **229**(14): 2626–2638, doi: 10.1177/0954406214562634.

7. LIU Y.Y., WANG L.Q., ZHU Z.C. (2016), Experimental and numerical studies on the effect of inlet pressure on cavitating flows in rotor pumps, *Journal of Engineering Research*, **4**(2): 19, doi: 10.7603/s40632-016-0019-x.

8. MARINARO G., FROSINA E., SENATORE A. (2021), A numerical analysis of an innovative flow ripple reduction method for external gear pumps, *Energies*, **14**(2): 471, doi: 10.3390/en14020471.

9. PASZKOWSKI W. (2020), Modeling of vibroacoustic phenomena using the method of parameterizing the audio signal, *Eksploatacja i Niezawodność – Maintenance and Reliability*, **22**(3): 501–507, doi: 10.17531/ein.2020.3.13.

10. TANG C., WANG Y.S., GAN J.H., GUO H. (2014), Fluid-sound coupling simulation and experimental validation for noise characteristics of a variable displacement external gear pump, *Noise Control Engineering Journal*, **62**(3): 123–131, doi: 10.3397/1/376212.

11. WANG H., DENG G., LI Q., KANG Q. (2016a), Research on bispectrum analysis of secondary feature for vehicle exterior noise based on nonnegative Tucker3 decomposition, *Eksploatacja i Niezawodność – Main-

tenance and Reliability, **18**(2): 291–298, doi: 10.17531/ein.2016.2.18.

12. WANG C.X., WU C.J., CHEN L.J., QIU C.L., XIONG J.S. (2016b), Review on mechanism and prediction of flow-induced noise [in Chinese], *Research on Chinese Ships*, **11**(1): 57–71.

13. WOO S., VACCA A. (2020), Experimental characterization and evaluation of the vibroacoustic field of hydraulic pumps: The case of an external gear pump, *Energies*, **13**(24): 6639, doi: 10.3390/EN13246639.

14. WOO S., VACCA A. (2022), An investigation of the vibration modes of an external gear pump through experiments and numerical modeling, *Energies*, **15**(3): 796, doi: 10.3390/EN15030796.

15. ZHANG D.S., ZHANG N.S., XU B., ZHAO R.J., GAO X.F., LI N. (2021), Numerical simulation of the flow-induced noise in a water-jet pump based on the Lighthill acoustic analogy theory [in Chinese], *Journal of Vibration and Shock*, **40**(10): 278–287.

16. ZHOU Y.K., LI W.W., YANG D.P. (2018), Noise simulation analysis of a variable displacement external gear pump and unloading groove optimization, *Open Access Library Journal*, **5**(11): 1–9, doi: 10.4236/oalib.1105030.